Resource expansion with uncertainty quantification of regolith-hosted REE deposits using radiometric data

Caers[1], J., Yin[1], D., Asadi[1], A., Carrasco-Rojas[2], M., Delgado-Rivas[2], D., Martin[2] J. and Mardonez[2], J.

[1]Mineral-X, Department of Earth & Planetary Sciences, Stanford University, USA

[2]Aclara Resources, Chile.

e-mails

"Jef Karel Caers" <jcaers@stanford.edu>

"David Zhen Yin" <yinzhen@stanford.edu>

"Adel Asadi" <aasadi1@stanford.edu>

"Mauricio Carrasco" <mauricio.carrasco@aclara-re.com>

"Diego Delgado" <diego.delgado@aclara-re.com>

"joaquin.mardonez@aclara-re.com" <joaquin.mardonez@aclara-re.com>

This is a non-peer reviewed preprint submitted to EarthArXiv.

Resource expansion with uncertainty quantification of regolith-hosted REE deposits using radiometric data

Caers[1], J., Yin[1], D., Asadi[1], A., Carrasco-Rojas[2], M., Delgado-Rivas[2], D., Martin[2] J. and Mardonez[2], J.

[1]Mineral-X, Department of Earth & Planetary Sciences, Stanford University, USA

[2]Aclara Resources, Chile.

Corresponding Author: Jef Caers, jcaers@stanford.edu, 450 Jane Stanford Way, Stanford, CA 94305, USA

Abstract

Rare earth elements (REE) are critical raw materials due to their essential role in modern technologies. In regolith-hosted REE (RH-REE) deposits a substantial fraction of the REE is present as ionically adsorbed, exchangeable cations on secondary clay minerals and amenable to mild extraction routes potentially being less environmentally disruptive than conventional hard-rock REE operations. Shallow drilling in combination with geophysical techniques are used to determine the potential of a regolith resource for economic extraction. In particular, airborne gamma-ray spectrometry provides indirect indicators of the regolith and parent lithology by mapping potassium, equivalent thorium (eTh) and equivalent uranium (eU) from low-altitude, line-spaced surveys. In a brownfield exploration context, neighboring densely drilled areas can be used as training sets to assess the potential undrilled areas. To do so, the flightline data needs to be interpolated to allow for correlation with REE concentration at borehole locations. In this paper, we show that the traditional methods of deterministic interpolation leads to an overly optimistic estimate of the REE concentration. As a solution, we propose a multi-variates stochastic simulation of the radiometric data in a Monte Carlo simulation framework. We illustrate the methodology with a case study from a RH-REE district in south-central Chile, located in the Coastal Range

about 15 km NE of Concepción. We show how the uncertainty approach identifies false positives created by deterministic interpolation and allows for a more accurate understanding of risk vs return in undrilled zones of the resource. Since the large majority of online available geophysical data are deterministically interpolated products, we also conjecture that our findings have wider implications for mineral prospectivity mapping involving geophysical and geological databases.

Keywords: REE deposits, Radiometric data, Geostatistics, Uncertainty Quantification

Key Message/highlights

- Deterministic interpolation of geophysical flightline data, correlated with borehole data leads to overestimation of resource potential
- A method of joint stochastic simulation of radiometric data alleviates this problem
- The approach is applied to a resource expansion of a REE deposit in Chile

Introduction

Rare earth elements (REE) are critical raw materials due to their essential role in modern technologies such as renewable energy, electronics, and advanced manufacturing. Among deposit types, regolith-hosted REE (RH-REE) deposits, also termed ion-adsorption clay deposits, are particularly distinctive. In these systems, a substantial fraction of the REE is present as ionically adsorbed, exchangeable cations on secondary clay minerals (e.g., kaolinite, halloysite, illite), a configuration often relatively enriched in HREE and readily amenable to mild extraction routes that can be operationally simpler and potentially less environmentally disruptive than conventional hard-rock REE operations. These systems form through prolonged weathering of felsic (commonly granitic) rocks, which liberates REE from accessory phases and leads to their adsorption within the regolith profile (Borst et al., 2020).

While RH-REE deposits are well documented in southern China, systematic exploration outside Asia is relatively recent, with most projects still in early stages; consequently, few mature occurrences are documented in the Western hemisphere (e.g., Borst et al., 2020; Sanematsu and Watanabe, 2016). Assessment is further hindered by practical disadvantages typical of lateritic settings, dense vegetation, pervasive soil and saprolite cover, high soil moisture, and thick regolith that reduce outcrops and obscure bedrock signals, together with strong vertical and lateral heterogeneity within weathering profiles that complicate extrapolation from sparse observations.

In this context, airborne gamma-ray spectrometry provides indirect indicators of the regolith and parent lithology by mapping potassium, equivalent thorium (eTh) and equivalent uranium (eU) from low-altitude, line-spaced surveys in which scintillation detectors record natural gamma photons emitted by near-surface soil (Minty, 2003; Roehrlich, 2025). Crucially, these measurements do not detect REE directly; their value lies in constraining the regolith framework and surface geology, while anomalies in thorium and uranium commonly relate to variations in lithology and refractory accessory minerals (e.g., monazite, xenotime, zircon); the signal is shallow and can be modulated by soil moisture, vegetation, and survey geometry, so it must be treated as an indirect, calibrated proxy (BEA, 1996; Dickson, 1995; Metelka et al., 2018; Wilford, 2012).

Typical to any airborne geophysical data, airborne gamma-ray spectrometry is collected along flightlines with data more frequently sampled along than across flightlines. The label data consists of boreholes along which concentration of REE are geochemically assessed, hence the data has a

very different geometry (sparse in the plane, dense in the vertical). Borehole locations, however, do not necessarily overlap with the flightline data. In our seminal contribution (Wang et al., 2020) we showed that a deterministic interpolation of geophysical data, or upscaling of label data to the geophysical scale to allow for the creation of a training set creates significant bias in resource or mineral potential estimates. This is because the interpolated maps have less variance than the actual geophysical data, thereby artificially increasing the correlation with the label data. Instead, we illustrated that uncertainty quantification through stochastic simulation, explicitly accounting for the interpolation uncertainty and data variability is needed to remove false positives created by the smooth interpolation, a property that we illustrate once again in this paper. Since then, other authors have expanded on the need for rigorous uncertainty quantification in all forms of mineral prospectivity mapping (Li et al., 2023; Lindi et al., 2024; Peng et al., 2023; Yang et al., 2024; Zhang et al., 2024; Zuo, 2017).

In this study, we propose a resource-assessment framework with explicit uncertainty quantification that fuses radiometric covariates with borehole geochemistry to assess regolith-based REE resources. We illustrate the methodology with a case study from a RH-REE district in south-central Chile, where the goal is to expand the resource beyond the current drilling program. Aclara Resources, a canadian REE mining company, provided the data to develop this study. The selected study area is called Penco district. Located in the Coastal Range ~15 km NE of Concepción within granitoids of the Southern Coastal Batholith, a Late Carboniferous–Early Permian calc-alkaline arc emplaced ca. 320–300 Ma (Deckart et al., 2014). The local bedrock consists primarily of I-type tonalite to granodiorite, with common accessory REE-bearing minerals (e.g monazite, xenotime, zircon and allanite) typical of felsic arc plutons and their metamorphic country rocks (BEA, 1996). These accessory phases constitute the primary REE reservoir and, during prolonged weathering, release REE into the weathering profile, where they are transported and adsorbed onto clay minerals within a subsurface, clay-rich horizon. Climatically, the humid temperate setting of the coastal belt in central-southern Chile, with high annual precipitation and persistent soil moisture, favors deep, chemically mature regolith developed on subdued topography (Garreaud et al., 2009). In humid-temperate to subtropical settings underlain by granitoid rocks, prolonged chemical weathering leads to intense leaching of feldspars and ferromagnesian phases, progressive kaolinization (formation of kaolinite-group clays), and vertical redistribution of dissolved species within the regolith. Under such conditions, REE released from accessory minerals are retained on

clay surfaces by ion-exchange, producing lateritic–saprolitic profiles that can reach tens of meters in thickness, which is a key precondition for ion-adsorption–type enrichment (Sanematsu and Watanabe, 2016; Wilford, 2012).

In this paper we intend to show the need quantify uncertainty in the interpolation of radiometric flightline data to assess REE resources. Since such data is multivariate, we intend to develop a multi-variate stochastic simulation method that is easy to use yet reduces the demonstrated bias of the traditional deterministic interpolation. We intend to show how in a real case study the traditional approach of ignoring uncertainty provide overly optimistic results, while the uncertainty approach provided a much clearer distinction in the selection of new target area for drilling.

Methodology

Methodology development on Synthetic case

To illustrate the methodology, we designed a synthetic case that has many elements in common with the actual case, while in the result section we cover the case study fully. Figure 1 presents three reference-truth maps that serve as reference truths: (i) a map of ΣREE (La–Lu ; Y) concentration derived from regolith borehole assays in the Penco district, analyzed by inductively coupled plasma–mass spectrometry (ICP–MS); and (ii–iii) maps of equivalent thorium and equivalent uranium derived from airborne gamma-ray spectrometry. The first map is built from whole-rock borehole geochemistry reported in parts per million, whereas the radiometric maps report equivalent concentrations, also in parts per million. For REE, we will use the harmonic mean of the borehole data, which we will motivate in the next section. From these maps, we can calculate any reference statistics such as variances and correlation coefficients.

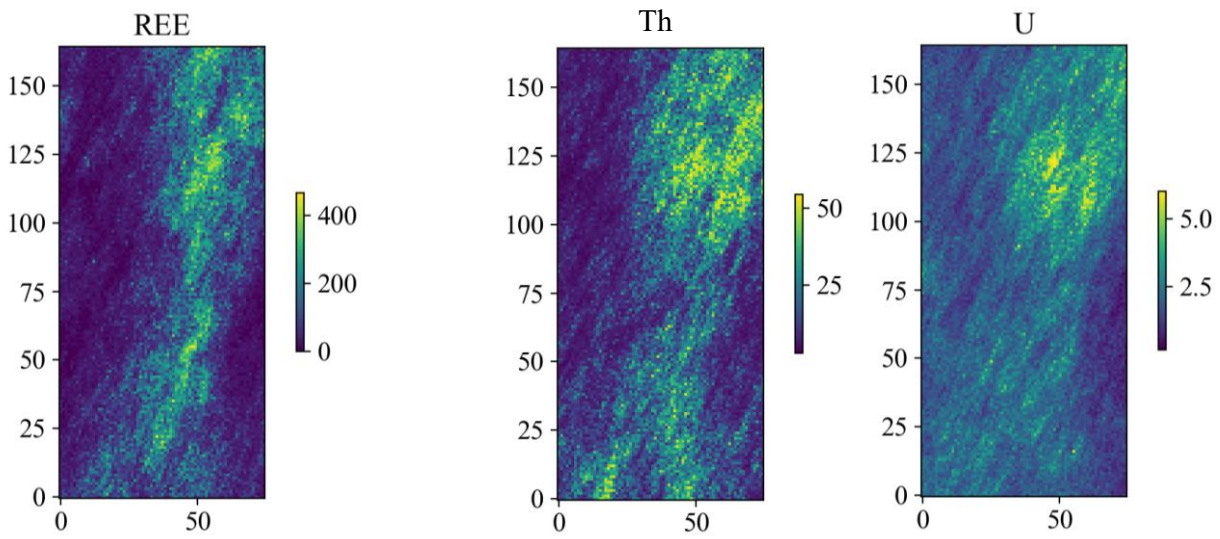

Figure 1: reference truth for the synthetic case. (left) the target to be predicted reference truth, (rightleft) the two predictors.

We mimic the data configuration of the actual case by extracting flightline data on thorium and uranium, as well as a set of borehole locations with observed harmonic mean, see Figure 2. In real cases (see later) boreholes are clustered in radiometric high. The aim now is to train a machine learning method that can be applied elsewhere. For simplicity, we will use logistic regression (LR) to predict the probability that the harmonic mean exceeds 200ppm. Logistic regression is a log-linear model that does not overfit data, so our evaluation criterion will be how well ML predicts the reference probability which is given in for thorium and for both thorium and uranium in Figure 3.

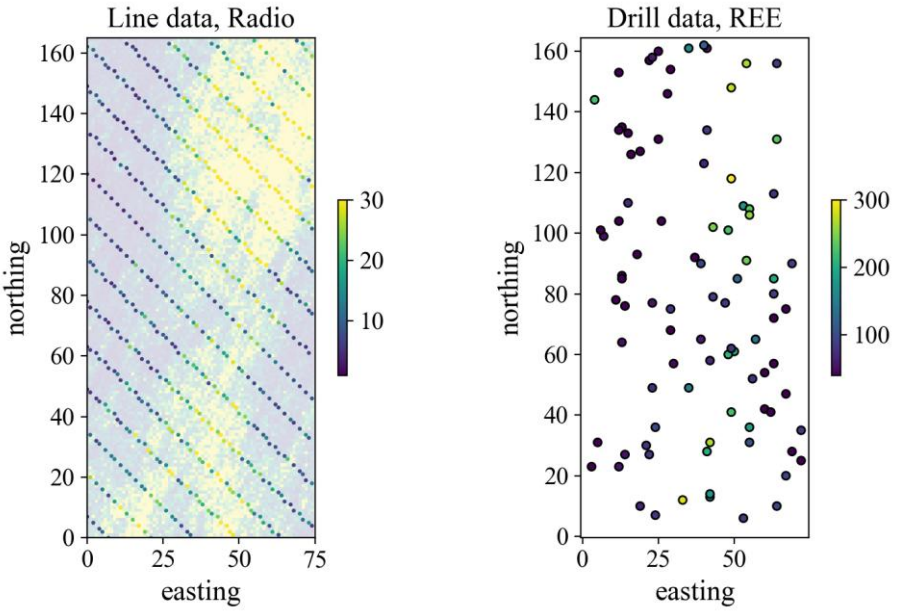

153

154 Figure 2: configuration of the flightline data and the drillhole data with observed harmonic mean

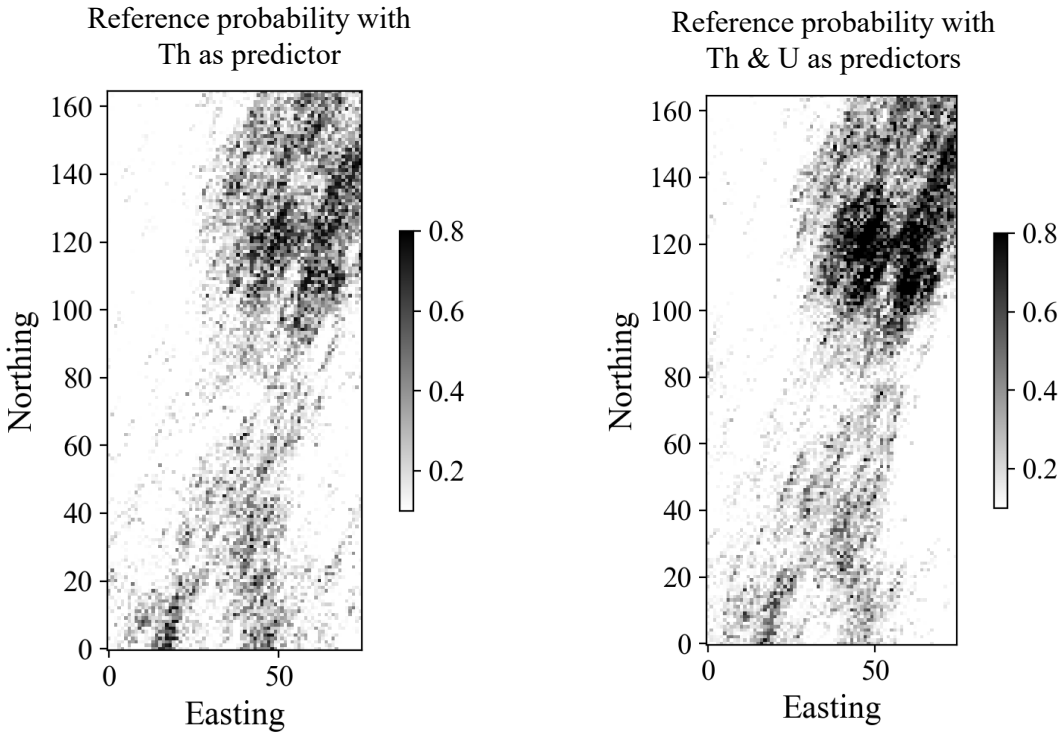

155

156 Figure 3: reference probability in case predictors are exhaustively measured, (left) for Th only, (right) for
157 both Th & U.

Problem formulation

Random function models

We consider a typical brownfield exploration problem, where substantial drilling and resource assessment has been done in Area X, and where the aim is to apply the learning to area Y, nearby, within the same mineral system. Our methodology is applicable to any combination of input datasets, such as geophysical, geological or geochemical, but we will consider first the availability of just one input dataset, one single predictor, d.

Before any machine learning between input and target output, we take a geostatistical approach defining random functions on all spatial variables. More specifically, we aim to generate multiple 2D realizations of the predictor d that preserves some measurable statistical properties, such as the variogram of the flightline data on d and the correlation with the borehole data.

In the case of RH-REE deposits, we need to define the target random function (the output). A challenge occurs in the sense that the resource consists of clay layers enriched with high concentration of REE. We propose to use the harmonic mean $h(x)$ as a vertical average at each location x of the deposit as the target (primary) random function and the single predictor as the secondary random function $d(x)$. . The use of the harmonic mean is motivated by the layered-ness of the RH-REE deposit system. Figure 4 illustrates how a harmonic mean can distinguish layers of high REE content, while other averages fail. A high harmonic mean entails the presence of layers highly concentrated in REE. Additionally, we can retrieve data on the harmonic mean at the borehole locations x_α, by harmonic averaging the 1D borehole data into a 2D map of harmonic average sample data. Later in the case study, we will illustrate how other properties such the probability of REE over some threshold can be predicted as well.

arithmetic mean	334.00	167.33	1	34.00
geometric mean	10.00	7.94	1	4.64
harmonic-mean	1.50	1.50	1	1.49

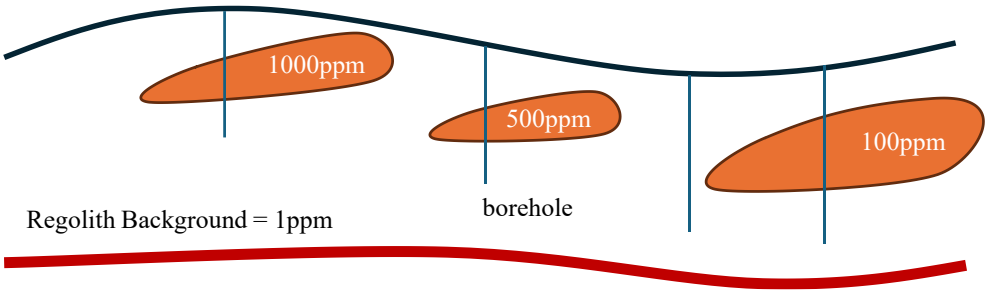

Figure 4: comparison between various ways of averaging borehole data. The harmonic mean is constant for all attractive cases of high REE concentration.

The predictor is also modeled as a random function, because its values are only known at limited flight line data point.

At area Y, we only observe data of the secondary random function, the flightline data.

To apply any machine learning algorithm, we need to complete the map of the secondary variable conditioned on the flightline data. That way, we can construct a training set. This requires modeling the flightline data at the same locations as the borehole data. The aim therefore is to interpolate the flightline data such that certain measurable statistical properties are maintained, namely:

- The interpolate flightline map needs to match the flightline data at their locations.
- The interpolated flightline map needs to have similar mean, variance and variogram as the flightline data.
- The interpolated map needs to have the same correlation coefficient with the borehole data as the estimated correlation coefficient.

In geostatistics, it has been established that there is no unique map since no metric of misfit with a reference truth is specified. Instead, conditional simulation is used ensure these statistical properties are preserved when sampling multiple simulated realizations. Here we use a Gaussian random function, which works well in terms of integrating linear correlations and are based on variograms. Many fast, sampling algorithms, such as sequential simulation can be used (Deutsch and Journel, 1998).

The remaining problem is inference of the correlation coefficient between flightline data and harmonic mean, because of the lack of co-located flightline and borehole data. Instead, we first estimate an omnidirectional cross-correlogram to estimate the relationship between the distance between any two flightline & harmonic mean data and the correlation coefficient:

$$\hat{\rho}(s) = \frac{1}{|N(s)|} \sum_{m,n}^{|N(s)|} \tilde{d}(x_n)\tilde{h}(x_m)$$

Eq. 1

with $\tilde{d}$ and $\tilde{h}$ the standardized harmonic mean and flightline data (mean = 0, variance =1)

$$N(s) = \{m, n | \|x_n - x_m\| = s\}$$

Eq. 2

and $|N(s)|$ its cardinality. To estimate this correlogram (see Figure 5), we create distance classes of h, and average over any pairs in the same distance class. The estimated correlogram coefficient between d and h is

$$\hat{\rho}_{dh} = \hat{\rho}(0)$$

Eq. 3

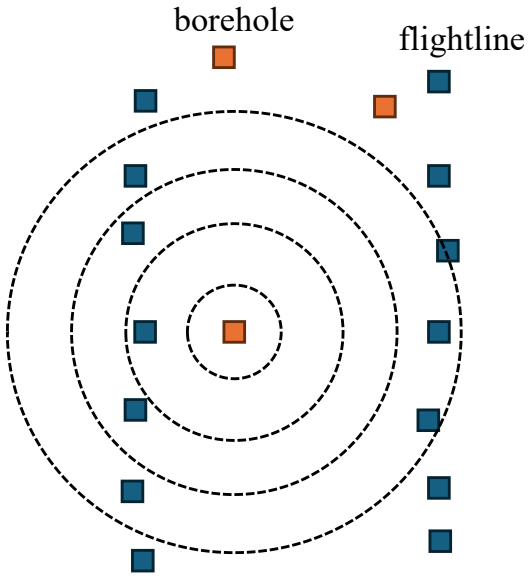

Figure 5: illustration of how to estimate the cross-correlogram. After standardizing each variable, pairs of observation are searched over the domain that are within the same distance class of each other. These distance classes are represented using concentric circles.

Co-simulation of the flightline data

In order to be able to correlate the flightline data with the borehole data, we need to simulate the flightline data at unsampled locations using flightline data as well as the known harmonic mean at borehole locations. The most common approach in geostatistics is to assume a Gaussian random function and estimate the parameters of the Gaussian distributions using co-kriging methods. However, full co-kriging methods are difficult to use when the number of variables increases (Goovaerts, 1997). It should be noted once more that the goal is not build a detailed resource model, but to complete the sparse flightline data into multiple simulated maps, that are to be used for something else: machine learning and application to other areas. An approximate, but simpler method extendable to many variables is to perform co-located co-kriging of the $d(x)$:

$$\hat{d}(x) = \sum_n w_n \, d(x_n) + v \, h(x)$$

Eq. 4

$d(x_n)$ is the flightline data at locations x, and $h(x)$ is the harmonic mean simulated at all locations x in the domain, w_n and v are the co-kriging weights. Using co-located data $h(x)$ only is a reasonable assumption knowing that the flightline data is much more densely sampled than boreholes. When using co-located co-kriging with Markov model 1 (Journel, 1999), we only need to specify the variogram of $d(x)$ and the correlation coefficient $\hat{\rho}_{dh}$, which was inferred using the cross-correlogram in the previous section. MM1 is an appropriate model when the primary variable (d) has less variation than the secondary variable (h).

We summarize the procedure before applying it to a synthetic example.

1. Estimate the cross-correlogram between the flightline data and the borehole harmonic mean data.
2. Use the cross-correlogram to estimate the correlation coefficient.
3. Estimate the 2D variogram of the borehole harmonic mean.
4. Estimate the 2D variogram of the flightline data.
5. Simulate the 2D harmonic mean conditioned to harmonic mean data

6. Using co-simulation of a Gaussian random function, simulate a realization of the flightline data using
    - The estimated variogram model of $d(x)$.
    - The estimated correlation coefficient between d & h.
    - The flightline data.

Multiple realizations are obtained by repeating step 5 & 6.

Illustration on synthetic case

We first set up the comparison base case, which is what is usually done: deterministic interpolation of the flightline data. Here we use kriging, but any methodology can be used. **Error! Reference s ource not found.** shows the interpolated Th and U data and the probability maps predicted using LR.

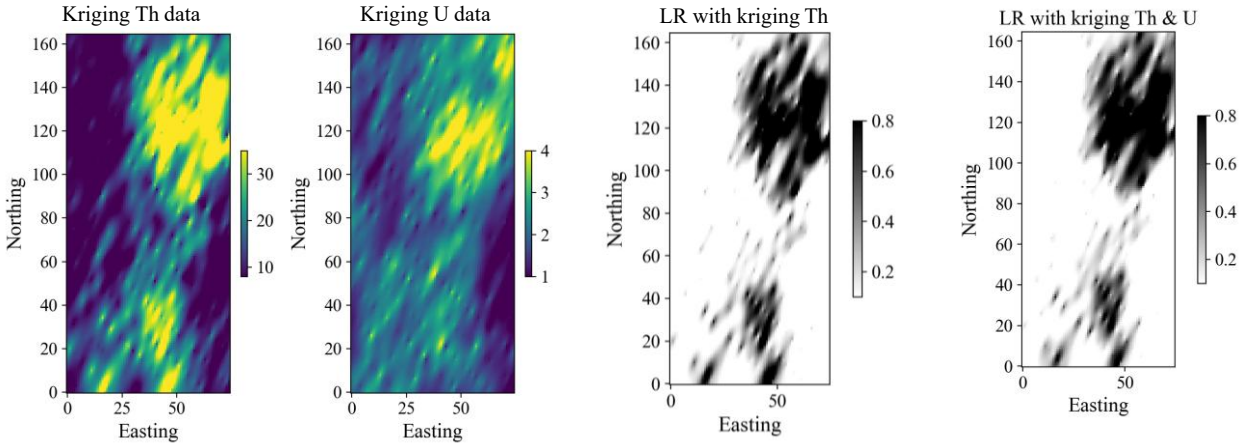

Figure 6: a traditional approach is to interpolate the geophysical data deterministically, then apply a machine learning approach to get a single map of predictions of REE-h.

However, when calculating the correlation coefficient between the kriged map and the borehole data (=0.67), see Figure 7, we notice a significant increase in correlation from the true correlation (=0.52), see Figure 7. Interpolators are also smoothers meaning that the interpolated maps have less variance than the actual data. The smoothing creates artificial correlation. Because of the increased correlation, the prediction is likely overly optimistic.

We now apply the above simulation approach which calls first for estimating the cross-correlogram. Extrapolating the cross-correlogram to lag distance = 0 we can estimate correlation coefficient to be ~ 0.51, which is very close to the actual correlation.

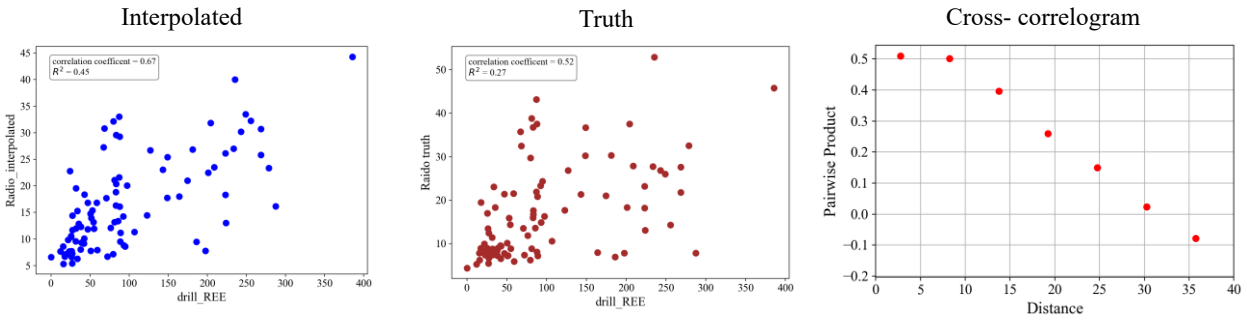

Figure 7: correlation coefficient between interpolated Th and REE vs correlation calculated from the truth, (right) the cross-correlogram between Th and REE.

The next steps in the above procedure is the generate multiple realizations of the REE constrained to borehole REE data, then co-simulation (using the MM1 model) of the Th data constrained to Th flightline data and the previously simulated REE, see **Error! Reference source not found.**. Using t he simulated Th data, we can run a logistic regression (LR) predictor on each map to get the corresponding probability. One notices that the resulting probability maps are much less smooth than the kriged probability maps. In Figure 9 we show the histogram of the LR regression coefficients on Th and compare it with the single LR regression coefficient obtained with kriging and the true value. Clearly, kriging results in overconfidence in the predictions (too high REE) while the simulation approach captures the true value.

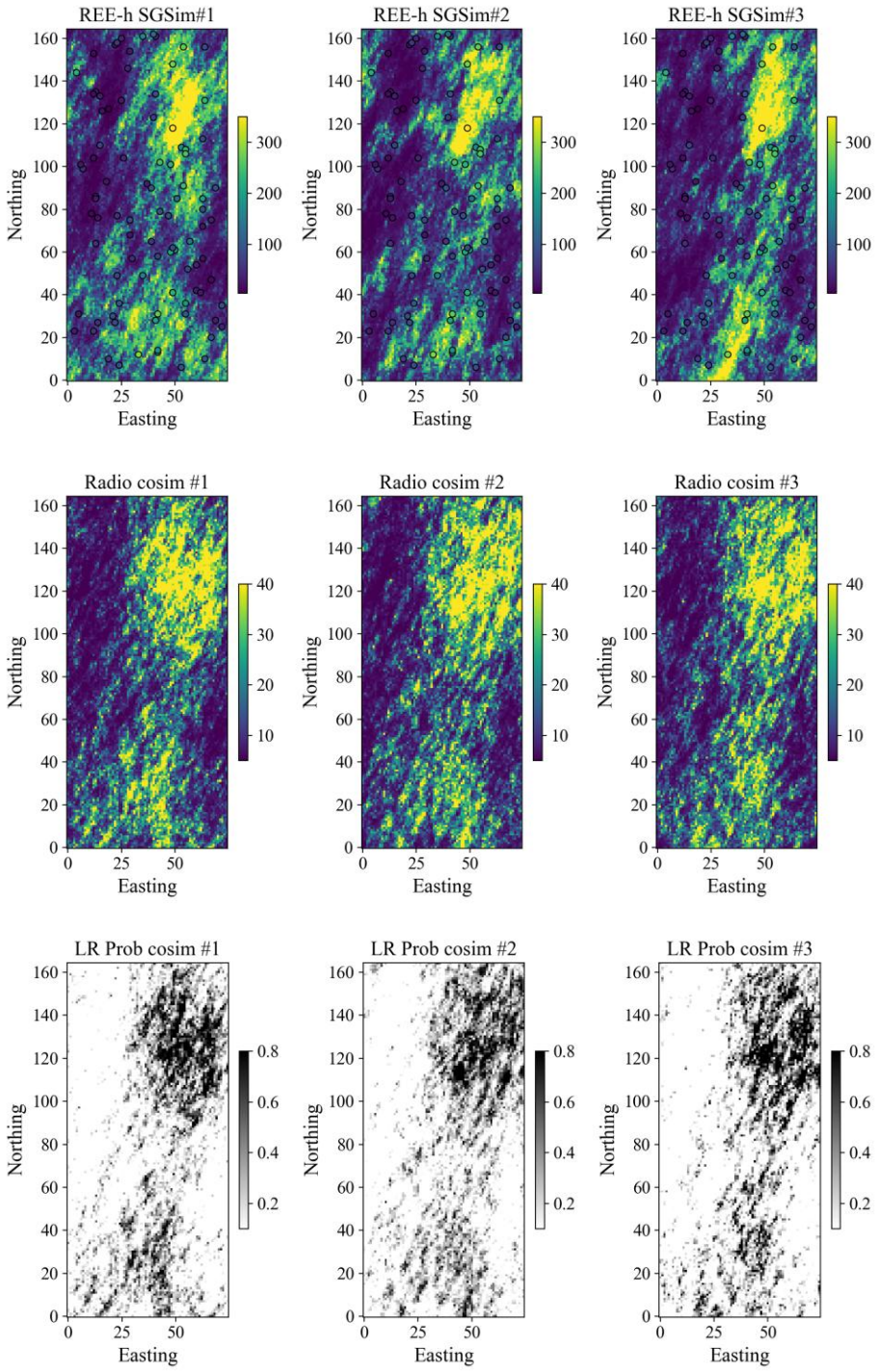

Figure 8: (top) simulated REE harmonic mean constrained to borehole data, (middle) co-simulated Th constrained to Th flightline data and previously simulated harmonic mean, (bottom) prediction of REE harmonic mean over the entire domain.

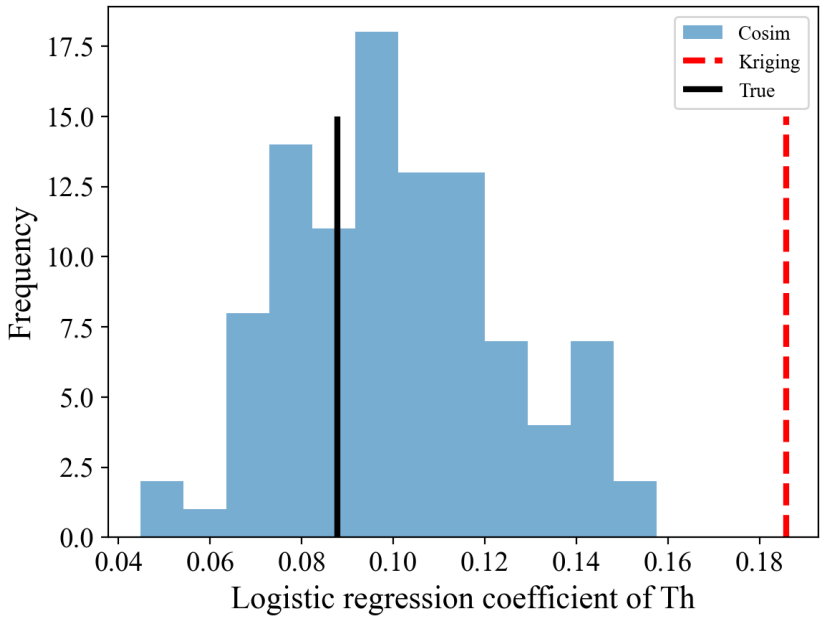

Figure 9: comparing the true logistic regression coefficient assigned to Th versus the kriging-based and simulation-based (histogram).

Extension by including additional data layers

We now present the extension to multiple variables. Again, we rely on a simplified approach that avoids the use of multiple cross-covariance modeling. Consider the case where we have K data layers data, $Z_1, Z_2, \ldots Z_K$ that require interpolation before they can be used in machine learning applications. Using the above procedure, we estimate the K correlation coefficients $\hat{\rho}_{z_k h}$ between borehole and flightline data. Additionally, we estimate the $K(K+1)/2$ correlation coefficients$\hat{\rho}_{z_k z_{k'}}$.

First, we assume a Markov assumption, namely that if Z_{*1} the most correlated data to the borehole data h, then we model Z_{*1} conditional to h as before (the * refers to a ranking with respect to some other variable). Next, consider Z_{*2}, the data that has the highest correlation with Z_{*1}, then we assume conditional independence, namely

$$F(Z_{*2}|Z_{*1}, h) = F(Z_{*2}|Z_{*1}) \qquad \text{Eq. 5}$$

F is the multivariate Gaussian distribution. Eq. 5 is a reasonable assumption since Z_{*1} already contains information on h, we can continue doing assuming at each step

$$F\left(Z_{*(k+1)}\middle|Z_{*k}, Z_{*(k-1)}\right) = F(Z_{*(k+1)}|Z_{*(k)})$$

The conditional independence is motivated by the fact that in linear methods, such as kriging, any data that has less correlation tends to be screened away (be redundant) by data with higher correlation.

Figure 10 when comparing with Figure 7, shows there is not much difference in correlation between REE and U, and REE vs Th. However, the U data looks noisier compared to Th (a known property in radiometric data), hence we do not expect U to provide much more additional prediction power, compared to using Th alone.

We perform co-simulation of U constrained by the U flightline data and the previously simulated Th realizations, and make predictions see Figure 11.

In Figure 12 we show the resulting LR predictions and the LR coefficients. Two effects can be noted 1) the LR gives too high weight to uranium compared to thorium, this is because of the limitation of the log-linear model assumption 2) the LR coefficient for Th lies outside the uncertainty band predicted with the simulation approach.

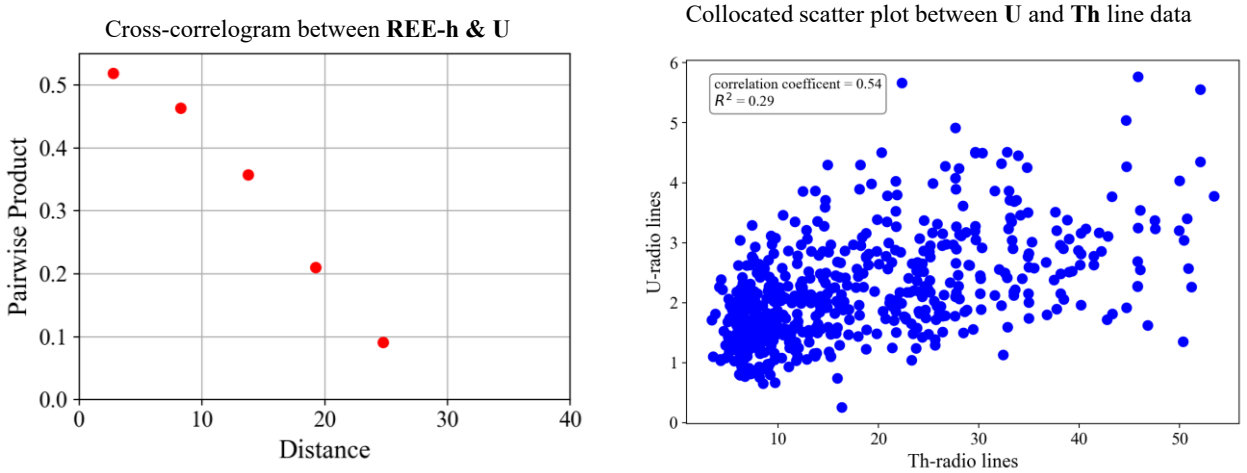

Figure 10: (left) cross correlogram between REE from boreholes and U from flightlines. (right) scatterplot between U and Th from flightline data.

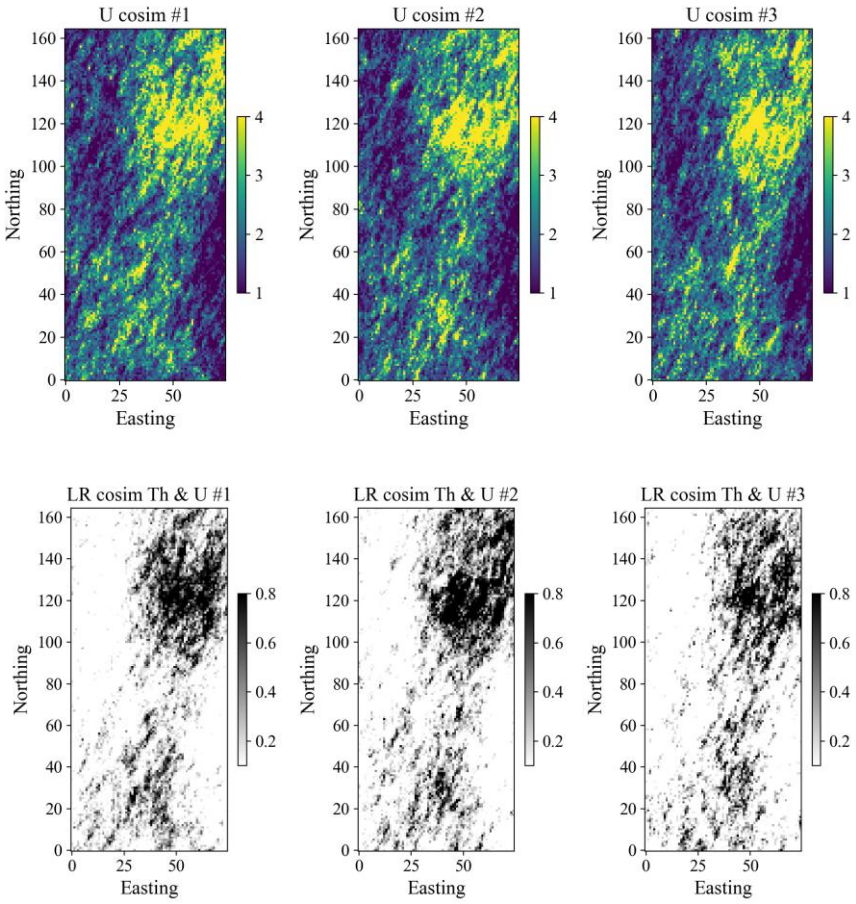

Figure 11: co-simulation of the U flightline data using previously simulated Th data. (bottom) prediction of REE-h using the simulated Th and U data.

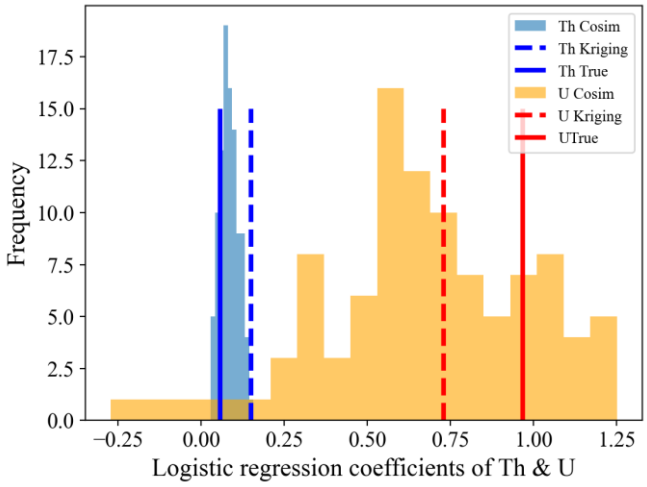

Figure 12: comparing the true logistic regression coefficient assigned to Th & U versus the kriging-based and simulation-based (histograms).

Resource expansion at Penco district

We now turn to the actual case and consider all three radiometric data: U, Th and Kp. Given the company's interest in conducting a preliminary, model-based screening of potential zones to support a future drilling campaign, we frame the following analysis as anexercise. Without asseing technical or operational feasibility. Using the training data (boreholes + simulated flightline data) our purpose is to predict REE concentrations in the undrilled target area indicated in the green box (see figure 13). In the Penco district, empirical evidence indicates that RH-REE occurrence is strongly related to lithological settings. Accordingly, we adopt an operational threshold of 1000 ppm ΣREE to distinguish the primary REE lithology from other district lithologies, which tyically exhibit lower REE concentrations. .

Hence, now we use the harmonic mean of the boreholes to simulate flightline data that honors correlation with the harmonic mean, while the prediction involves establishing an ML model that predicts the probability of being above 1000ppm given the flightline data. In Figure 13 we show the binary indicator, which equals one when any value in the borehole exceeds 1000ppm and zero else.

The procedure follows the template of the synthetic case. Here is the full Monte Carlo workflow:

In the training area

- Simulate one realization (i) of $REE - h$ constrained to borehole data and $REE - h$ variogram
- Define the order of simulation of (Th, U, Kp)
- Simulate (in order of maximal correlation) one realization (i) of Th, U, Kp constrained to flightline data and their respective variograms
- Extract training data consisting of binary indicators $REE > 1000ppm$ as target and Th, U, Kp at borehole locations as predictors
- Run a machine learning model to predict $P_{(i)}(REE > 1000\ ppm|Th, U, Kp)$

In the target area

- Simulate (in order of maximal correlation) one realization: Th_i, U_i, Kp_i The correlation between REE-Th = 0.81, REE-U = 0.68, REE-Kp = 0.28.

- Apply the machine learning model to estimate $P_{(i)}(REE > 1000\ ppm|Th_i, U_i, Kp_i)$

Repeat these steps for multiple realizations i

Aggregate all the predictions $P_{(i)}(REE > 1000\ ppm|Th_i, U_i, Kp_i)$ into a single prediction $P(REE > 1000\ ppm|Th, U, Kp)$.

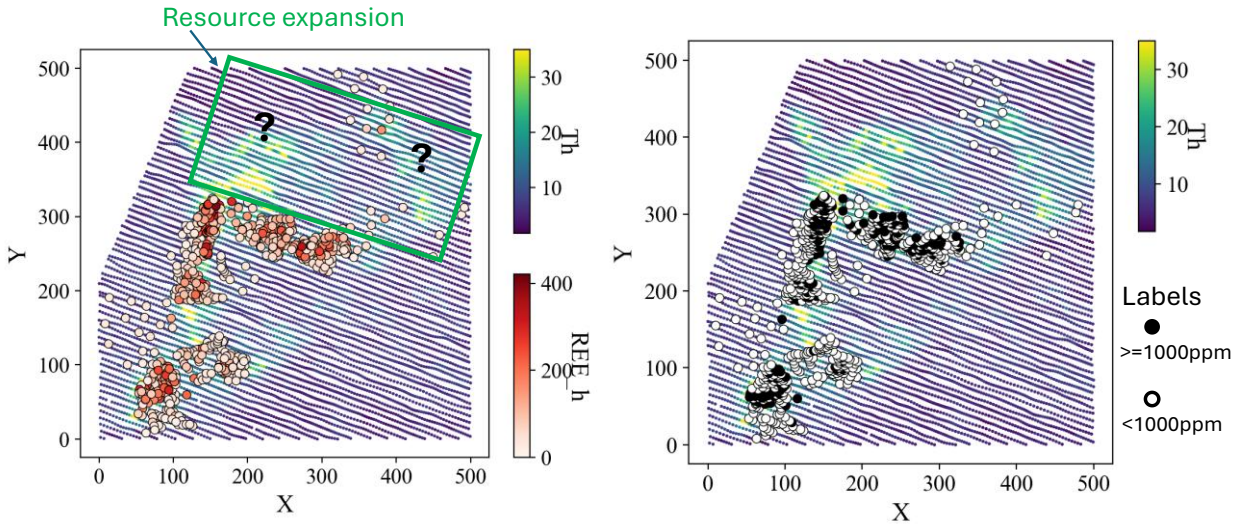

Figure 13: the target is to expand the resource from the drilled areas into the green box. (left) the harmonic mean at boreholes and flightline data (Th), (right) locations where REE concentration exceeds 1000ppm.

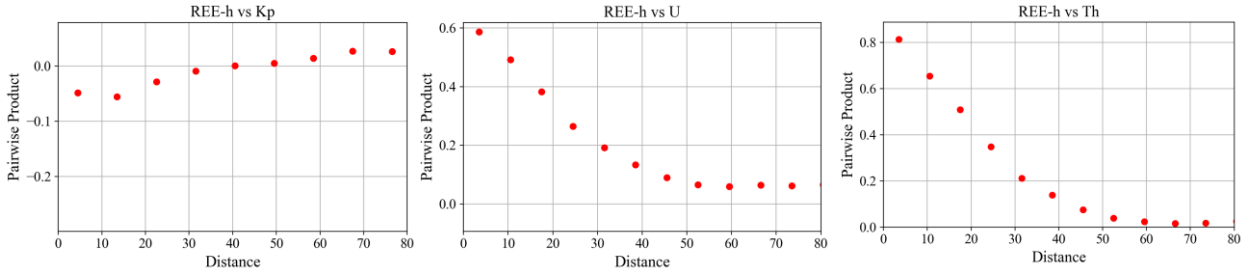

Figure 14: cross-correlograms between REE-h and Kp, U and Th.

Th correlated to REE-h

U correlated to Th

Kp correlated to on U

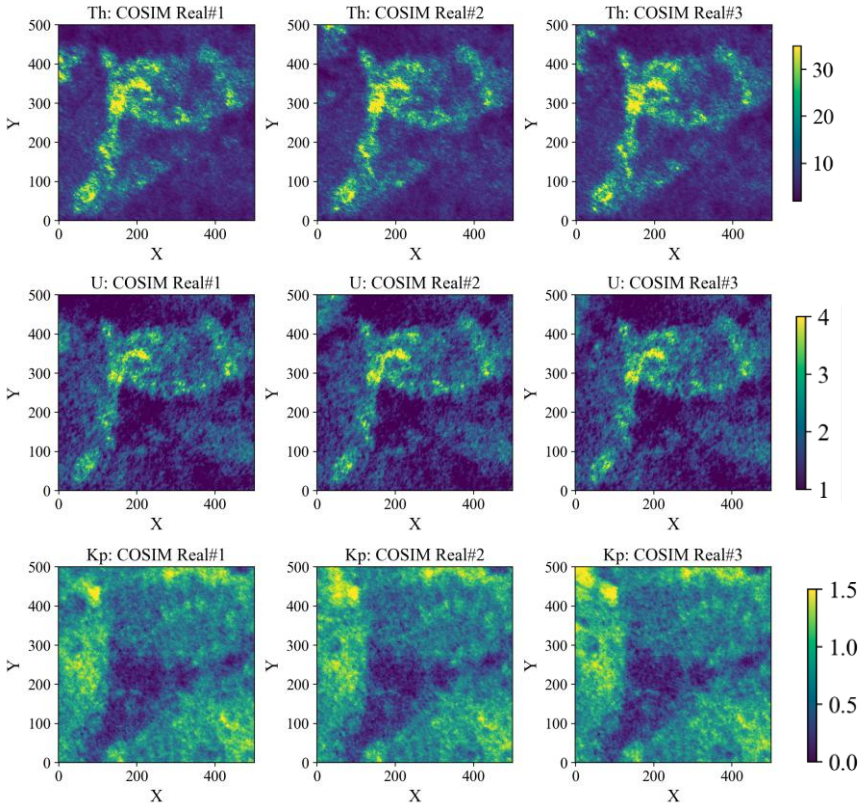

374

375 Figure 15: Three realizations of the simulated flightline data

376

377

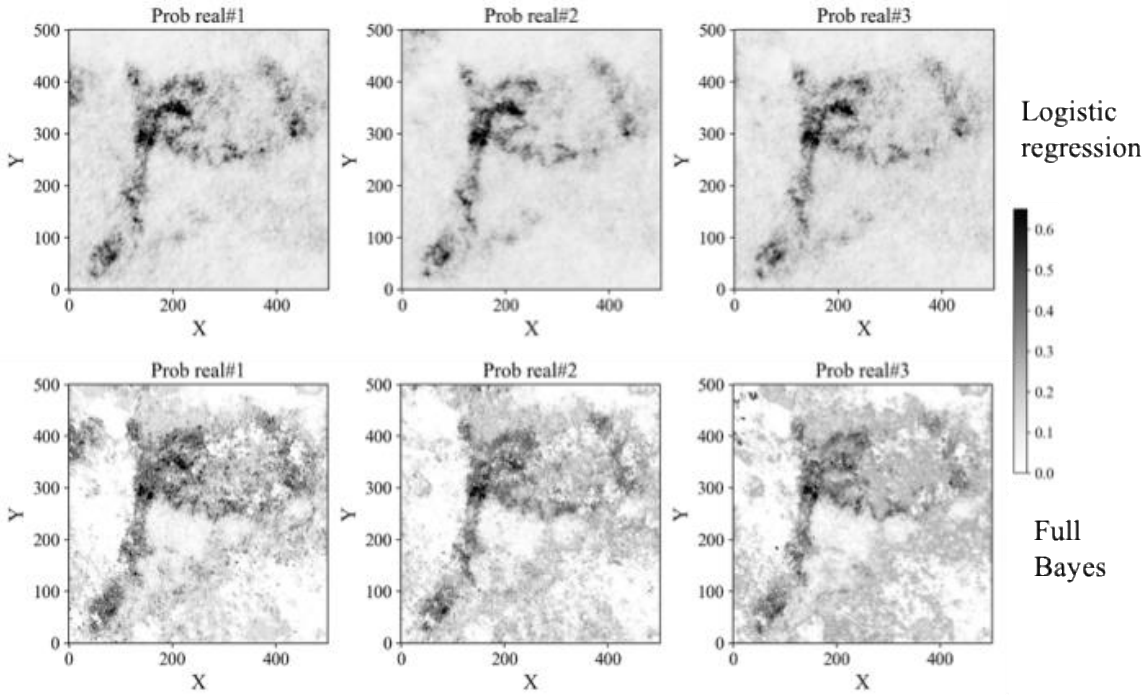

Figure 16: (top) Logistic regression of P(REE>1000) given flightline data over the entire domain shown for three realizations, (bottom) using the full Bayes approach.

In Figure 1Figure 14, we observe the cross-correlograms between REE-h and Th, U, Kp, note that Kp has basically no correlation with REE-h. Based on this information, we generate multiple realizations of Th, U, Kp through co-simulation. These co-simulation realizations are then used to predict $P(REE > 1000ppm|Th, U, Kp)$, first using a LR regression model and then using a full Bayesian approach (Figure 16). In the latter we use Bayes rule $P(REE > 1000ppm|Th, U, Kp) \sim f(Th, U, Kp|REE > 1000ppm)P(REE > 1000ppm)$

Eq. 6

where the 3D likelihood f is estimated using kernel density estimation (Wang et al., 2023). The full Bayes approach is possible because we only have three predictors and a sufficient number of boreholes.

We generated an ensemble of 100 realizations of probability maps. This allows us to further calculate the *return* and *risk* (Wang et al., 2020) to interpret the Monte Carlo realizations of probability at each location **x** for decision making:

$$return(\mathbf{x}) = \overline{logO} = \frac{1}{L}\sum_{\ell=1}^{L} logO\left(P\left(\mathbf{x}^{(\ell)}\right)\right)$$

Eq. 7

$$risk(\mathbf{x}) = \frac{1}{L-1}\sum_{\ell=1}^{L}\left(logO\left(P\left(\mathbf{x}^{(\ell)}\right)\right) - \overline{logO}\right)^2$$

Eq.8

Here L is the number of realizations and $p^{(\ell)}(\mathbf{x})$ is the probability at a location $\mathbf{x}$ on the grid for realization number ℓ. $logO(P) = log\left(\frac{P}{1-P}\right)$ is the log odd ratio of the probability P at each location. Figure 17 bottom figures show the *return* and *risk* maps. Figure 17 top further plots on the x-axis increasing *return*, while on the y-axis decreasing *risk*, where each dots represent a location grid. The efficient frontier (blue circles) shows the locations where *risk* and *return* can be traded off. We find 11 locations on the *risk* vs *return* plot the efficient frontier. These locations are shown on the return map of Figure 17 bottom. They can be used as feasible choices for future drilling with making tradeoffs. For instance, the tangent point (red rectangular) can be regarded as the optimal location for the next drilling.

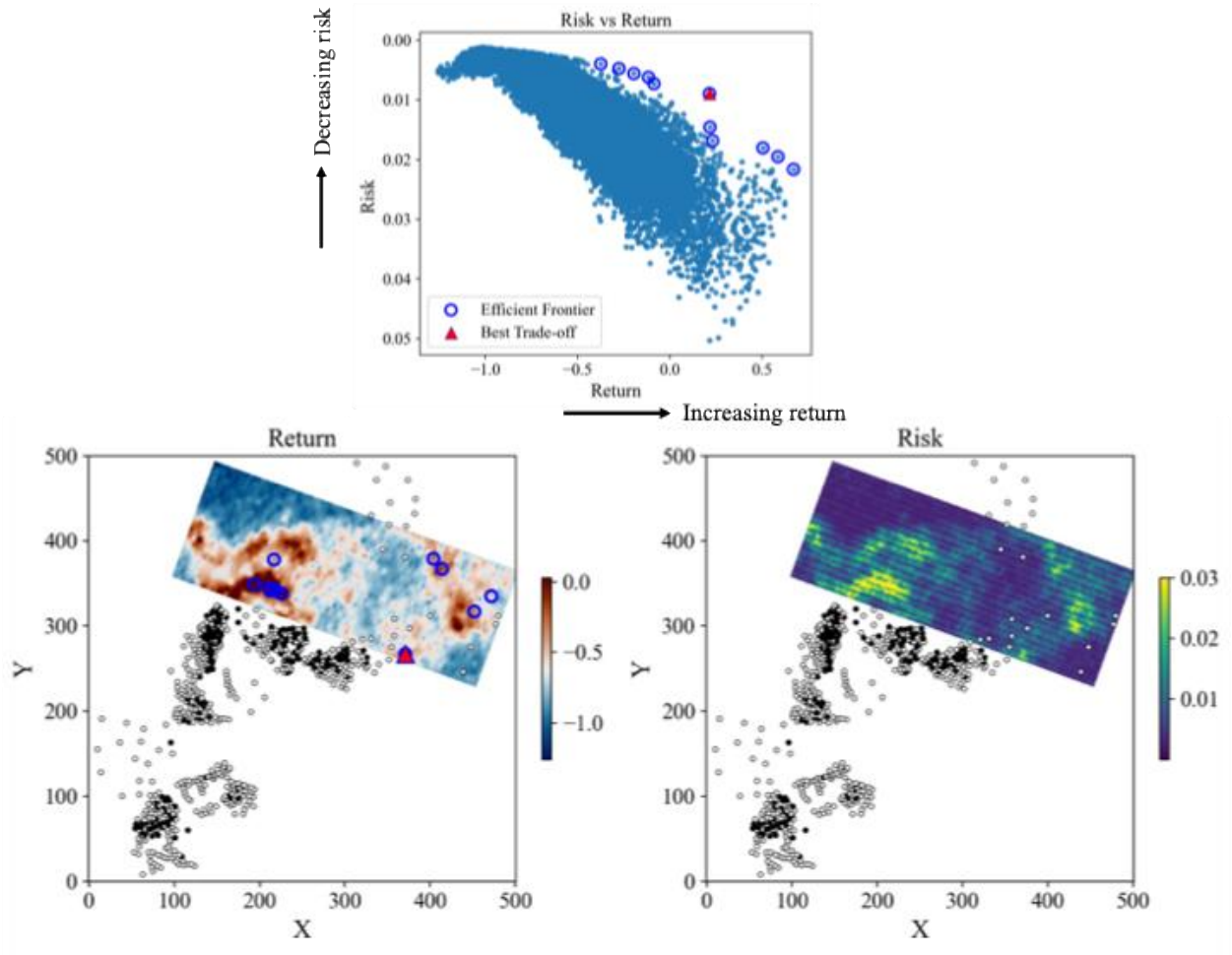

Figure 17: (top) plotting the increase *return* for $P(REE > 1000ppm)$ versus decreasing risks. The blue circles are the efficient frontier with the red rectangular as the best trade-off option. (bottom) return and risk juxtaposed to drill-hole locations corresponding to the efficient frontier.

Conclusions

In this paper, we provide a stochastic approach to evaluate the possibility of resource expansion in a regolith-hosted REE deposit, based on nearby drilling and airborne radiometric data. The key contribution is the stochastic co-simulation of the radiometric data that allows creating datasets for machine learning approaches. We demonstrate that the usual deterministic interpolation creates significant bias in the prediction because of the smoothing of data, creating an artificially higher correlation with the REE concentration. For that reason, the approach is relevant to other similar

problem where airborne geophysical data is used in conjunction with data at much higher resolution, such as drilling or outcrop sampling.

Acknowledgments

We thanks members of the Mineral-X industrial affiliates program for funding this work.

Statement and Declarations

Conflict of Interests: the authors declare that they have no known competing financial interests or personal relationships that could have appeared to influence the work reported in this paper.

References

BEA, F., 1996. Residence of REE, Y, Th and U in Granites and Crustal Protoliths; Implications for the Chemistry of Crustal Melts. Journal of Petrology 37, 521–552. https://doi.org/10.1093/petrology/37.3.521

Borst, A.M., Smith, M.P., Finch, A.A., Estrade, G., Villanova-de-Benavent, C., Nason, P., Marquis, E., Horsburgh, N.J., Goodenough, K.M., Xu, C., Kynický, J., Geraki, K., 2020. Adsorption of rare earth elements in regolith-hosted clay deposits. Nature Communications 11. https://doi.org/10.1038/s41467-020-17801-5

Deckart, K., Hervé, F., Fanning, C.M., Ramírez, V., Calderón, M., Godoy, E., 2014. Geocronología U-Pb e isótopos de Hf-O en circones del batolito de la Costa Pensilvaniana, Chile. Andean Geology 41. https://doi.org/10.5027/andgeov41n1-a03

Deutsch, C.V., Journel, A.G., 1998. GSLIB: Geostatistical Software Library and User's Guide. Oxford University Press.

Dickson, B.L., 1995. Uranium-series disequilibrium in Australian soils and its effect on aerial gamma-ray surveys. Journal of Geochemical Exploration 54, 177–186. https://doi.org/10.1016/0375-6742(95)00032-1

Garreaud, R.D., Vuille, M., Compagnucci, R., Marengo, J., 2009. Present-day South American climate. Palaeogeography, Palaeoclimatology, Palaeoecology 281, 180–195. https://doi.org/10.1016/j.palaeo.2007.10.032

Goovaerts, P., 1997. Geostatistics for Natural Resources Evaluation. Oxford University Press.

Journel, A.G., 1999. Markov Models for Cross-Covariances. Mathematical Geology 31, 955–964. https://doi.org/10.1023/a:1007553013388

Li, N., Yin, S., Li, Cangbai, Wang, Y., Xiao, K., Cao, R., Hua, W., Chu, W., Song, X., Li, Cheng, 2023. An Uncertainty Analysis Method Based on a Globally Optimal Truth Discovery

Model for Mineral Prospectivity Mapping. Mathematical Geosciences 56, 249–278. https://doi.org/10.1007/s11004-023-10086-6
Lindi, O.T., Aladejare, A.E., Ozoji, T.M., Ranta, J.-P., 2024. Uncertainty Quantification in Mineral Resource Estimation. Natural Resources Research 33, 2503–2526. https://doi.org/10.1007/s11053-024-10394-6
Metelka, V., Baratoux, L., Jessell, M.W., Barth, A., Ježek, J., Naba, S., 2018. Automated regolith landform mapping using airborne geophysics and remote sensing data, Burkina Faso, West Africa. Remote Sensing of Environment 204, 964–978. https://doi.org/10.1016/j.rse.2017.08.004
Minty, B., 2003. Accurate noise reduction for airborne gamma-ray spectrometry. Exploration Geophysics 34, 207–215. https://doi.org/10.1071/eg03207
Peng, Q., Wang, Z., Wang, G., Zhang, W., Chen, Z., Liu, X., 2023. 3D Mineral Prospectivity Mapping from 3D Geological Models Using Return–Risk Analysis and Machine Learning on Imbalance Data. Minerals 13, 1384. https://doi.org/10.3390/min13111384
Roehrlich, E., 2025. International Atomic Energy Agency (IAEA), in: International Atomic Energy Agency (IAEA). Routledge. https://doi.org/10.4324/9780367199838-recw8-1
Sanematsu, K., Watanabe, Y., 2016. Characteristics and Genesis of Ion Adsorption-Type Rare Earth Element Deposits. Rare Earth and Critical Elements in Ore Deposits. https://doi.org/10.5382/rev.18.03
Wang, L., Yin, Z., Caers, J., 2023. Data Science for the Geosciences. Cambridge University Press.
Wang, Z., Yin, Z., Caers, J., Zuo, R., 2020. A Monte Carlo-based framework for risk-return analysis in mineral prospectivity mapping. Geoscience Frontiers 11, 2297–2308. https://doi.org/10.1016/j.gsf.2020.02.010
Wilford, J., 2012. A weathering intensity index for the Australian continent using airborne gamma-ray spectrometry and digital terrain analysis. Geoderma 183–184, 124–142. https://doi.org/10.1016/j.geoderma.2010.12.022
Yang, F., Zuo, R., Kreuzer, O.P., 2024. Artificial intelligence for mineral exploration: A review and perspectives on future directions from data science. Earth-Science Reviews 258, 104941. https://doi.org/10.1016/j.earscirev.2024.104941
Zhang, Z., Wang, G., Carranza, E.J.M., Du, J., Li, Y., Liu, X., Su, Y., 2024. An Uncertainty-Quantification Machine Learning Framework for Data-Driven Three-Dimensional Mineral Prospectivity Mapping. Natural Resources Research 33, 1393–1411. https://doi.org/10.1007/s11053-024-10349-x
Zuo, R., 2017. Machine Learning of Mineralization-Related Geochemical Anomalies: A Review of Potential Methods. Natural Resources Research 26, 457–464. https://doi.org/10.1007/s11053-017-9345-4